Philosophical Magazine
Vol. 89, Nos. 28–30, 1–21 October 2009, 2541–2555

Taylor & Francis
Taylor & Francis Group

Insights and challenges toward understanding the electronic properties of hydrogenated nanocrystalline silicon

Peter Hugger[a]*, J. David Cohen[a], Baojie Yan[b], Jeffrey Yang[b] and Subhendu Guha[b]

[a]*Department of Physics, University of Oregon, Eugene, OR 97405, USA;*
[b]*United Solar Ovonic LLC, 1100 W. Maple Road, Troy, MI 48084, USA*

(*Received 7 January 2009; final version received 19 February 2009*)

Hydrogenated nanocrystalline silicon (nc-Si:H) is a complex mixed-phase material containing regions of silicon nanocrystallites interspersed with amorphous silicon. It is an important material in efforts to advance the production of more economical multijunction thin-film silicon-based photovoltaic technologies. We have applied the junction capacitance methods of transient photocapacitance spectroscopy and drive-level capacitance profiling to understand its fundamental electronic properties. We compare results in both the annealed and light-soaked states for nc-Si:H samples having a wide range of amorphous-to-crystallite volume fractions. Significant differences between samples with lower and higher amorphous fractions are observed and we propose a tentative microscopic model that may account for these differences.

Keywords: nc-Si:H; micromorph; mixed phase; a-Si:H; amorphous silicon; defects; electronic properties; nanocrystals; photovoltaics; silicon-based materials; thin-film solar cells

1. Introduction

In the early 1970s, Walter Spear and his co-workers clearly demonstrated the enormous promise of the newly discovered non-crystalline form of silicon (hydrogenated amorphous silicon a-Si:H) as this material could be doped by adding phosphorous or boron impurities in a manner similar to crystalline silicon [1]. This result was quite unexpected at the time because the more familiar non-crystalline chalcogenide semiconductors could not be doped effectively. It became immediately clear that one could fabricate useful semiconducting devices from this material, and work on a-Si:H soon completely dominated the interest of workers in the non-crystalline semiconductor field, including considerable efforts to understand its electronic properties. Walter Spear and his collaborators, Pete LeComber and Arun Madan, were active in this effort, publishing a first working version of the density of states across the mobility gap in a-Si:H based upon their detailed studies of a-Si:H field effect transistors [2,3]. These state distributions were greatly revised over the next decade as many alternative experimental methods were applied to this

*Corresponding author. Email: phugger@uoregon.edu

ISSN 1478–6435 print/ISSN 1478–6443 online

DOI: 10.1080/14786430902886928
http://www.informaworld.com

problem, leading to a period of intense intellectual debate in which Walter Spear was a key contributor.

Junction capacitance techniques, such as admittance spectroscopy [4,5], capacitance voltage (CV) methods [6], and deep-level transient spectroscopy (DLTS) [7,8], played a crucial role in identifying the dominant defect levels to obtain a more accurate picture of the density of states. In the mid 1980s, two related techniques were developed that have since proven particularly useful in the study of disordered thin-film semiconducting materials: (1) the drive-level capacitance profiling (DLCP) method [9–12], and (2) transient photocapacitance spectroscopy [13–15]. Both of these methods have been applied extensively to the study of a-Si:H [9,10,15,16] and its alloys with germanium (a-Si, Ge:H) [17–19], and provide direct information on the thermal and optical transitions associated with deep defects. In contrast to methods that require specially prepared samples on particular types of substrates, junction capacitance methods are particularly useful in the study of photovoltaic devices as they can be applied to the semiconducting layer in its natural 'working' environment, such as a p-i junction or a Schottky diode.

Over the past decade, interest has been growing in another disordered thin-film form of silicon: hydrogenated nanocrystalline silicon, nc-Si:H. This material is being evaluated for use in multijunction solar cell devices as the low optical gap component in multijunction devices employing a-Si:H as the wide gap component (and, in some cases, utilize the a-Si, Ge:H alloys as an intermediate bandgap component) [20–24]. In one respect, nc-Si:H can be considered to be the form of microcrystalline silicon with the smallest crystallite sizes (typically about 20 nm) and, indeed, its optical properties closely resemble those of microcrystalline silicon, with an energy absorption edge near 1.1 eV. However, the best cell performance parameters have been achieved when this material is deposited very close to the amorphous/crystalline silicon phase transition [25–27], so that it actually becomes a truly mixed-phase material containing a significant volume fraction of a-Si:H, ranging from 20 to over 50%, as determined by Raman spectroscopy.

The record stabilized efficiency for a-Si:H based cells is currently held by a triple junction cell using nc-Si:H as its bottom (lowest gap) device [28]. This underscores the potential importance of this material for the future development of a-Si:H-based solar cell technologies. In this paper, we will summarize some of the insights we have obtained through the application of our junction capacitance methods to this problem. We are fortunate to have a great deal of experience in this regard, with a collection of experimental methods that have previously been very successful in elucidating the electronic properties of a-Si:H and the a-Si, Ge:H alloys. Unfortunately, the interpretation of the results from these measurements has not been nearly as straightforward as their application to these purely amorphous materials. This, we believe, reflects its basic nature as a complex mixed-phase form of silicon, which presents an entirely new set of challenges in trying to map out its basic electronic properties. As these complex issues will undoubtedly continue to be the subject of intense debate over the next several years, it is reminiscent of those debates concerning a-Si:H 25 to 30 years ago. We are certain that Walter Spear would have enjoyed it.

2. Samples

As mentioned in Section 1, junction capacitance-based experimental methods, utilized in our studies, are performed directly on solar cell devices in their working configuration. The results to be presented here were obtained from a series of sample devices incorporating an undoped nc-Si:H absorber layer deposited at United Solar. In most cases, the structure was stainless steel/n^+/i(nc-Si:H)/p^+/ITO, where the nc-Si:H absorber layers were deposited using an RF or modified VHF (MVHF) glow discharge (PECVD) process. The results discussed in this paper were taken for the sample devices listed in Table 1. Sample 14657 was fabricated in a unique configuration, in which, to reduce any post-deposition oxygen contamination, the nc-Si:H layer was sandwiched between 200-nm layers of a-Si:H. A few films (for example 13993) were prepared on textured Ag/ZnO substrates to facilitate light-trapping. Film thicknesses were typically 500–1500 nm.

To study the effects of crystallinity on the electronic properties of these devices, the nc-Si:H films were deposited under conditions to produce a material of varying crystallite content across the entire area of the substrate. An array of semi-transparent 0.05 cm^2 ITO top contacts were then deposited on the completed device, yielding a set of co-deposited solar cells of varying amorphous volume fraction, X_a.

The amorphous fraction for each device, given in Table 1, was estimated using Raman spectroscopy. These spectra were obtained using a Renishaw RM series confocal Raman microscope with a 785-nm (1.58 eV) excitation laser. This choice of wavelength meant that the light would be both well absorbed by the nanocrystallite component in these films and would also penetrate deep into the nc-Si:H i-layer to yield an amorphous volume fraction representing a spatial average over most of its active region [29]. Each Raman spectrum was baseline-corrected at 400 and 550 cm^{-1}, then deconvolved into three peaks: two Gaussian peaks representing the a-Si:H TO mode centered near 480 cm^{-1} and the intermediate peak located near 510 cm^{-1}. A third peak centered near 520 cm^{-1}, representing the c-Si TO mode was fit with a mixed Gaussian/Lorenztian distribution whose mixing constant was employed as an additional fitting parameter. Amorphous volume fractions were then calculated

Table 1. Samples for which data are presented in this report. Except for sample 14657, all were actual solar cells and their performance parameters are listed. The amorphous volume fractions, X_a, were estimated using Raman spectroscopy and have an estimated systematic error of ±0.05.

Sample	X_a	nc-Si:H i-layer thickness (μm)	V_{oc} (V)	J_{SC} (mA/cm^2)	Fill factor	Efficiency (%)
13993	0.47	1.1	0.548	24.39	0.641	8.57
14036	0.37	1.2	0.448	17.38	0.568	4.42
15125-74	0.28	1.5	0.501	14.89	0.529	3.95
15125-94	0.64	1.4	0.597	11.86	0.496	4.31
16114	0.71	0.9	0.568	14.73	0.651	5.4
16115	0.23	2.8	0.470	19.4	0.449	4.1
14657	0.54	0.7	N/A	N/A	N/A	N/A

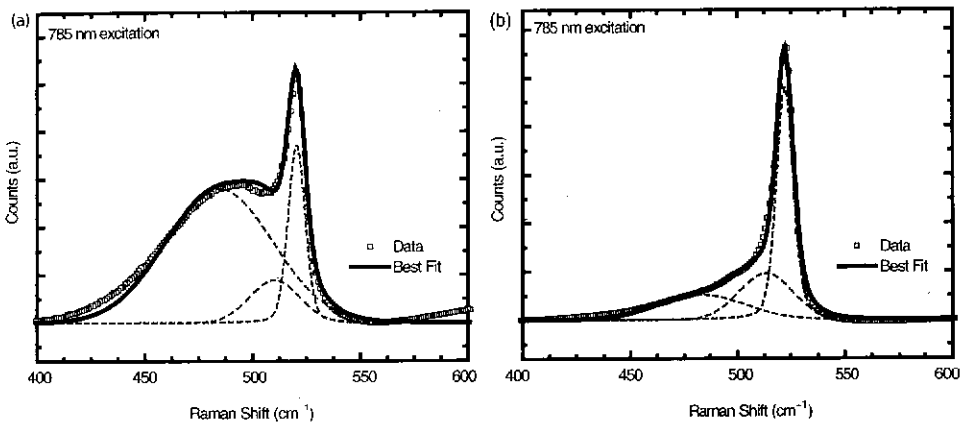

Figure 1. Typical Raman spectra obtained from nc-Si:H samples. (a) A spectrum exhibiting a large amorphous component, and (b) one with a large crystalline component. Using the integrated intensities of the deconvolved peaks (dashed lines), the amorphous volume fractions were determined to be 0.71 ± 0.05 and 0.23 ± 0.05, respectively.

by taking ratios of these integrated peak intensities using an additional correction factor to account for the different optical cross-sections of a-Si:H and the microcrystallites [30,31]. The same correction factor was used in the Raman analysis for all samples. Figure 1a shows a Raman spectrum for a highly amorphous device (sample 16114) which typifies spectra for low crystalline volume fraction devices. Likewise, Figure 1b shows a Raman spectrum for a primarily crystalline device (sample 16115), typical of the spectra for high crystallinity devices. In both cases, the component peaks used to fit the data are shown by the dashed lines.

3. Transient photocapacitance and photocurrent methods

3.1. *Description of measurements*

The transient photocapacitance (TPC) method yields optical spectra similar to those obtained for any absorption measurement method that can access the sub-bandgap density of states with sufficient sensitivity, such as CPM [32,33] or PDS [34]. However, the TPC method records the optically induced changes in the junction capacitance, which indicates a photo-induced change in charge within the depletion region. This TPC signal will be positive if majority carriers (electrons) predominantly leave the depletion region during the measurement, but negative if minority carriers (holes) are predominantly released. This means that TPC has the ability to distinguish carrier type. Detailed descriptions of the TPC method have been given previously [13,14,35], where [13] and [14] provide good descriptions of the effects of all possible optical transitions on the TPC signal, and [35] provides an excellent discussion of transient photocharge measurements in general.

To briefly outline the TPC method, the effect of a monochromatic optical excitation on the junction capacitance is observed over a measurement time window lasting ~1 s. Working carefully in a linear optical excitation regime, the capacitance

response to this optical excitation is measured and normalized to the photon flux. Because the sign of the TPC signal depends on the predominant type of carriers collected during the measurement time window, we have

$$\text{Signal}_{\text{TPC}} = K(n - p), \tag{1}$$

where n and p represent the total number of collected electrons and holes, respectively. The scale factor K depends on measurement temperature, the time-window of observation, the DC bias applied across the barrier junction, measurement frequency and the ambient charge distribution across the depletion region. All of these quantities are generally kept constant during the acquisition of a TPC spectrum.

A method closely related to the TPC method described above is the transient photocurrent (or TPI) method. This is carried out in an identical way except that the junction photocurrent produced during the measurement is recorded instead of the capacitance. Because currents resulting from either electrons or holes escaping the depletion region have the same sign, we then have

$$\text{Signal}_{\text{TPI}} = K'(n + p). \tag{2}$$

In a sense, the TPI spectrum provides a 'theoretical maximum' version of the TPC spectrum in that it reveals roughly how the TPC spectrum would appear if there were zero minority carrier collection to diminish the TPC signal magnitude. Indeed, if only majority carriers can be collected, then the TPI and TPC spectra should appear identical (except for a simple scale factor), provided we are examining a spatially uniform sample.

Therefore, when the TPC and TPI spectra are correctly scaled relative to each other, the two measurements can be used to estimate the minority carrier collection fraction by taking the ratio of properly scaled spectra, $R = \text{Signal}_{\text{TPC}}/\text{Signal}_{\text{TPI}}$:

$$f_p = f_n \frac{1 - R}{1 + R}, \tag{3}$$

where $f_p = p/(n+p)$ and $f_n = n/(n+p)$. We generally assume that, due to their much higher mobilities, the collection fraction for electrons will have a value close to unity.

3.2. *Results from photocapacitance and photocurrent*

A key result we obtained in applying these methods to nc-Si:H is that the relative degree of hole versus electron collection as a function of photon energy depends on the amorphous content of the film and is also greatly influenced by the degree of light soaking. 'Light soaking' refers to prolonged exposure of the device to 300 mW/cm^2, 610-nm long-pass filtered white light for 100 h. Figure 2 compares sets of TPC spectra obtained for two nc-Si:H sample devices with very different amorphous volume fractions. Figure 2a displays such spectra for a sample with a relatively low amorphous fraction. At the lowest measurement temperature, these spectra resemble those obtained from PDS measurements for microcrystalline Si in other laboratories [36,37]. As the temperature is increased, we observe that the signal intensity above the crystalline Si bandgap (1.1 eV) decreases monotonically.

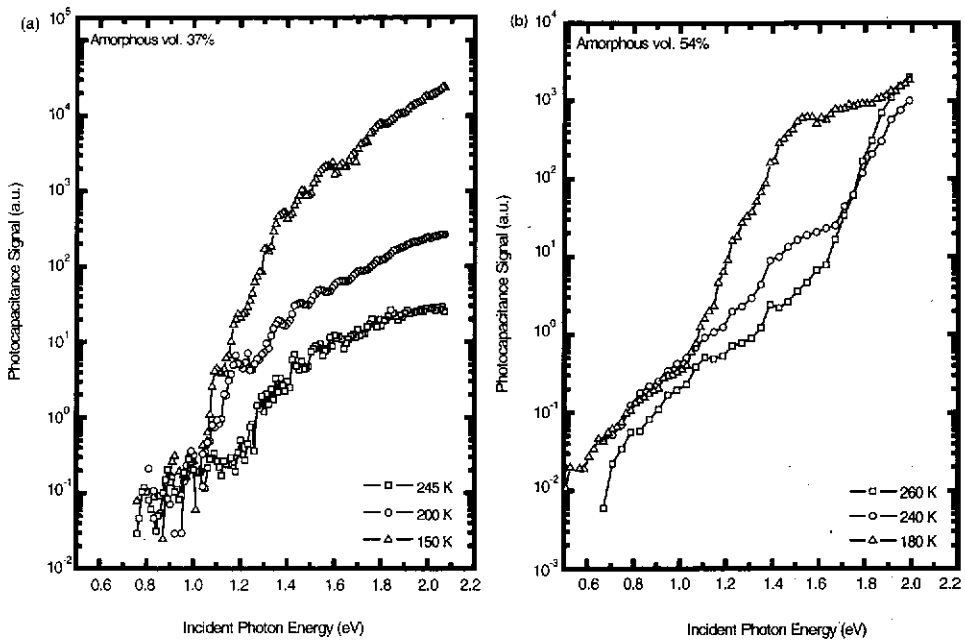

Figure 2. Typical photocapacitance (TPC) spectra versus temperature for two nc-Si:H samples in their annealed state. The nominally high degree of hole collection in each sample decreases with decreasing temperature. (a) The more nanocrystalline film (14036) shows little evidence of the a-Si:H optical bandgap, (b) while the more amorphous film (14657) reveals the a-Si:H band edge near 1.8 eV.

This is due to the nature of the photocapacitance signal, discussed in the above section, which reveals the difference between the electrons and holes collected. Thus, while photons with energies exceeding 1.1 eV excite equal numbers of electrons and holes, they are not collected with equal efficiency, and this means there is residual charge left in the depletion region over the timescale of the observed capacitance response. The positive sign of the TPC signal in Figure 2a indicates that the holes are being collected less efficiently than the electrons, but that this asymmetry decreases with increasing temperature. Thus, the TPC signal above 1.1 eV becomes smaller as the temperature is increased. Indeed, from auxiliary TPI measurements on this sample, we estimate that, at optical energy 1.5 eV, the relative hole collection (compared to that of the electrons) over the 1-s measurement window increases from less than 70% at 150 K to over 99% at 245 K.

Figure 2b shows a set of corresponding spectra taken for a sample with a higher amorphous Si fraction, published a few years ago [38]. The lowest temperature spectrum is qualitatively identical to those found in Figure 2a and to the optical spectra obtained by methods such as CPM and PDS for nc-Si:H materials. We again see a comparable increase in hole collection efficiency with increasing temperature above 1.1 eV, indicated by the decrease in the TPC signal in this energy regime. However, as the TPC signal decreases, it then reveals a residual spectrum that closely resembles that of hydrogenated amorphous silicon [11,14]. As argued in [38], this

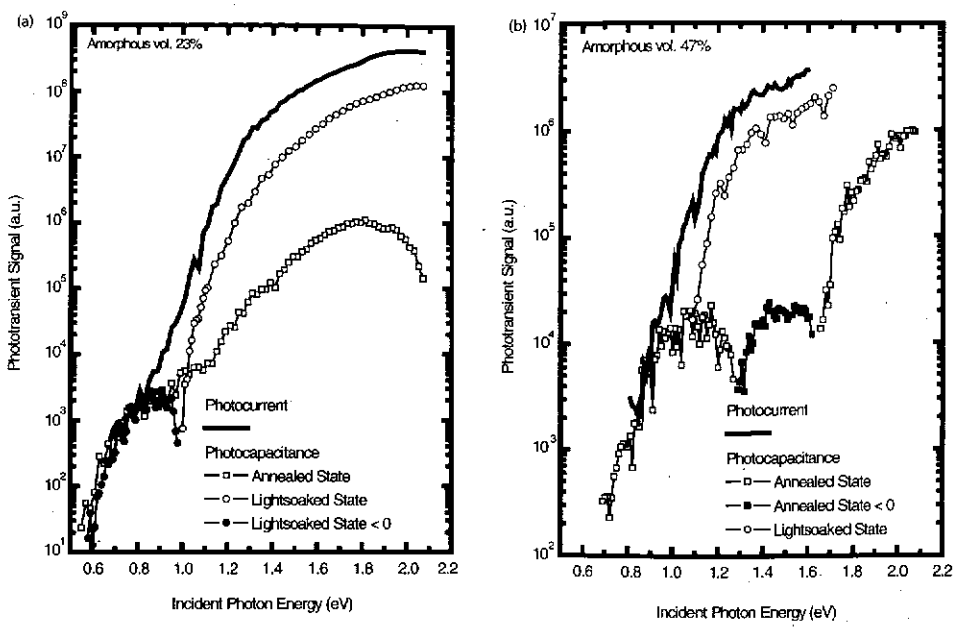

Figure 3. Photocapacitance (TPC) and photocurrent (TPI) spectra for two nc-Si:H samples in both their annealed and light-soaked states. The ratio of the TPI to TPC signals above 1.1 eV indicates the degree of hole collection. (a) The highly nanocrystalline film (16115) shows little evidence of the a-Si:H optical bandgap. In its light-soaked state, the negative TPC signal near $E \sim 0.6$ eV indicates unfilled defect states above the Fermi level. Spectra were taken at 325 K. (b) A more amorphous film (13993) reveals the a-Si:H band edge near 1.7 eV. At high temperatures (295 K), a negative TPC feature appears near 1.2 eV.

indicates a well-defined amorphous silicon phase within this sample, which actually maintains its microscopic identity with respect to its optical excitation spectrum. In this higher temperature regime, we believe that, because the hole collection in the amorphous silicon component is lower than the nanocrystalline silicon component, the amorphous silicon component dominates the appearance of the overall TPC spectrum (that is, TPC signal in the nanocrystalline phase above 1.1 eV has been greatly suppressed by its very high hole collection fraction).

Figure 3 compares the TPC and TPI optical spectra near room temperature for two additional nc-Si:H samples, again with higher and lower nanocrystallite fractions. Here, however, we display spectra both in the annealed state and after light soaking. First, we note that in both cases the TPI (photocurrent) spectra closely resemble the familiar absorption curve for micro-crystalline silicon and are essentially the same as the lower temperature TPC spectra for the two samples shown in Figure 2; namely, the optical bandgap for these materials is roughly 1.1 eV and there exists a band of deep defects at energies below 0.9 eV. The factor of ~200 suppression of TPC relative to TPI above 1.4 eV for both samples indicates that at least 99% of the minority carriers are being collected for every majority carrier over the measurement's 1-s timescale in the higher temperature regime. However, following light soaking, the TPC signal above 1.1 eV increases significantly implying

that the relative hole collection has dramatically decreased to below 90% in both cases. This behavior after light soaking has been universally observed for all the United Solar nc-Si:H we have examined by these methods.

Secondly, as in the comparison shown in Figure 2, the nc-Si:H film with the higher amorphous Si fraction shows a distinct amorphous phase in its TPC spectrum above 285 K, while this behavior is missing for the sample with the higher nanocrystalline fraction. Thus, qualitatively, the results for these two samples are similar for the two cases displayed in Figure 2. However, they also show a behavior not present in the spectra displayed in Figure 2; namely, regions in which the TPC signal actually becomes negative (the region with filled symbols). Such a negative signal in TPC is the signature of an optical transition between a valence band state and a deep empty gap state where the excited charge can remain trapped during the timescale of the measurement (see [39] for a more detailed discussion). In such a case, if the residual valence band hole escapes the depletion region, this results in a net negative residual charge in the depletion region as a result of the optical excitation and we, thus, observe a negative TPC signal.

Note that the negative features in the TPC spectra occur over different optical energy regimes for these two samples with greater and lesser nanocrystalline components. Also, no such negative features occur in the spectra for the two samples in Figure 2. This presents a rather significant challenge in the study of nc-Si:H materials; namely, how to account in a reasonably straightforward fashion for the great variety of behaviors exhibited by the optical spectra for these four samples.

The schematic band diagram in Figure 4 provides a possible solution. Optical transitions that might occur between the valence band and empty states of a defect band residing in the amorphous silicon phase region of the material are shown. Both transitions are of the type that may result in a negative TPC signal. Figure 4a illustrates a material with a lower fraction amorphous silicon component and, thus, narrower amorphous regions. In this case, the energy levels in the amorphous and crystalline phases are likely to be well mixed quantum mechanically (represented by the stippling in the figure). In such a material, the energy threshold for the optical transition shown reflects the energy difference between the top of the valence band in the crystallite and the defect energy. Figure 4b, on the other hand, illustrates a situation where the amorphous region has a larger spatial extent so that the spatial overlap (and corresponding matrix element) between the crystallite valence band state and the defect level in the amorphous region is small. In this case, the energy threshold would reflect the energy difference between the valence band states in the amorphous phase and the defect level. This transition energy will be larger by roughly the energy of the valence band offsets between the two phases. Indeed, from the negative TPC signal regimes in Figure 3, the difference in thresholds is 0.5–0.6 eV, roughly the valence band offset between crystalline and amorphous silicon as determined by several studies [40–42].

If this explanation is correct, then why are there no such negative signal regions in the TPC spectra in Figure 2? Probably because observing a net negative TPC response requires three conditions that must be met simultaneously:

(a) There must be a large unoccupied defect band in the depletion region that is still deep enough so that electrons inserted into it are not thermally re-emitted into the conduction band too rapidly. (b) One must be able to collect the residual hole in

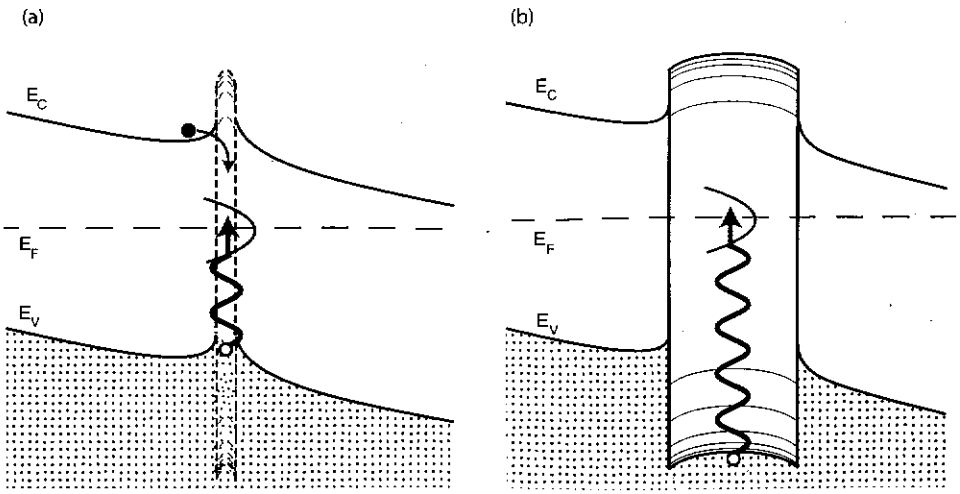

Figure 4. Possible optical transitions corresponding to the prominent negative features in the optical spectra from Figure 3. In a low amorphous fraction sample depicted for case (a), the threshold for a negative TPC signal will occur near 0.6 eV, while in a high amorphous fraction sample corresponding to case (b), the threshold might lie close to 1.2 eV due to the lack of close quantum mechanical coupling between the amorphous and crystalline phases. This diagram also suggests how electron trapping from the conduction band into a deep state occurs easily in case (a), while being largely suppressed in case (b).

the valence band with reasonable efficiency. (c) Transitions from filled gap states into the conduction band occurring over the same photon energy regime (which result in a positive TPC signal) must not be so strong that they overwhelm the transitions responsible for the negative signals.

Thus, the lack of a negative TPC regime for the more crystalline fraction sample in Figure 2 is probably a result of item (a) listed above; that is, the lack of a sufficiently large empty defect band. Indeed, the more crystalline sample in Figure 3 did not exhibit a negative feature until after it was light-soaked. Likewise, the lack of a net negative signal for the more amorphous sample in Figure 2 is likely due to (c): the presence of a strong transition from filled gap states into the conduction band. It might also be due to a lower hole collection fraction in that sample. Indeed, the negative region for the more amorphous sample in Figure 3 also disappears at a 20 K lower temperature due to decreases in hole collection.

In summary, the observation of a negative TPC signal provides an unambiguous signature of a valence band transition into an empty defect level. However, the lack of that signature does not mean the transition is absent, only that other factors make it difficult to observe. Therefore, we believe that the two spectra shown in Figure 3 provide clear evidence for a distinct crossover in the electronic properties of nc-Si:H with greater or lesser degrees of crystallinity. The model shown schematically in Figure 4 gives one attractive interpretation of these results and this observation is further strengthened by some of the DLCP results described in the following section.

4. Drive-level capacitance profiling

4.1. *Description of measurement*

Drive-level capacitance profiling (DLCP) is one of the most powerful techniques for learning about majority carrier traps in disordered materials because it can reveal both the energy and spatial distribution of such defects. It has been discussed in greater detail elsewhere [12]. Put simply, drive-level profiling is closely related to the more familiar C–V profiling method in which the junction capacitance is measured as a function of applied dc bias voltage, V. That dependence can be directly inverted to provide the doping profile in semiconducting materials containing negligible concentrations of deep defects. However, for semiconductors that do contain a large density of deep defects, the CV method is problematic since the charge density changes not only at the edge of the depletion region but also where energy levels of the deeper defects cross the quasi-Fermi level, well inside the depletion region. That deeper charge response is also very dependent on the timescale (ac frequency) used for the measurement.

In the DLCP method, instead of measuring the junction capacitance using a single value of the oscillating voltage amplitude, δV, one employs a series of increasing values to determine the first couple coefficients in the non-linear relation:

$$\mathrm{d}Q/\mathrm{d}V = C_0 + C_1\delta V + C_2(\delta V)^2 + \cdots$$

This behavior is partially governed by the thermal emission cutoff energy, E_e, which depends on the measurement (angular) frequency ω and temperature T:

$$E_e = k_B T \ln\left(\frac{\nu}{\omega}\right). \tag{4}$$

Here, ν is the usual thermal emission prefactor for the deep gap state response, which has been found to have a value of $\sim 2 \times 10^{13}$ s in a-Si:H [43–45]. Energy E_e describes how far below the conduction band edge defect states are able to respond dynamically at the measurement frequency ω.

Using the above parameters, the DLCP density becomes, in terms of the fundamental charge q, and the permittivity of the material ε:

$$N_{\mathrm{DL}}(x, E_e) = -\frac{C_0^3}{2q\varepsilon A^2 C_1} = n + \int_{E_C - E_e}^{E_F} g(E, x)\mathrm{d}E, \tag{5}$$

where n is the density of free carriers, A is the area of the device and $g(E, x)$ is the density of states within the gap at position x. Note that the integration is performed over gap states that are filled in the undepleted portion of the semiconductor but whose occupation is modulated within the depletion region down to the emission cutoff energy E_e. This density is then plotted as a function of $\langle x \rangle \equiv \varepsilon A/C_0$ (as in C–V profiling) as the dc bias is changed to reveal the spatial distribution of defects across the semiconductor.

4.2. *Results from drive level profiling*

The results from our DLCP measurements on nc-Si:H samples display even more consistent differences, depending on their amorphous volume fractions, than in the

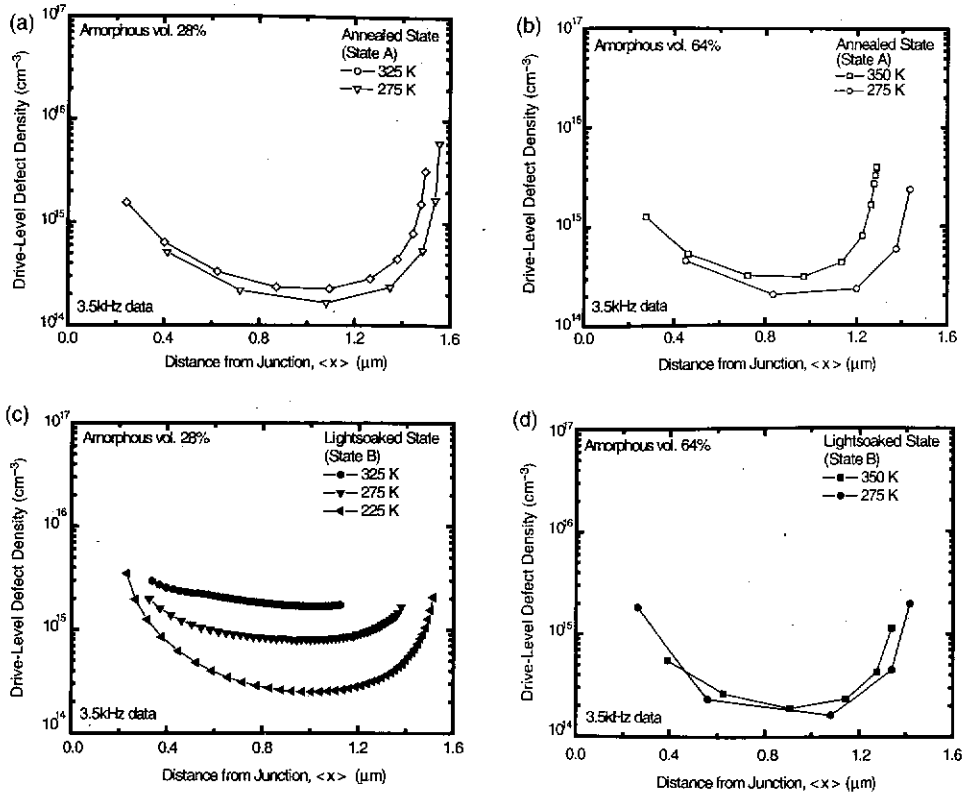

Figure 5. Typical DLCP results for samples of very different amorphous content. Respectively, (a) and (c) show the annealed state (State A) and the light-soaked state (State B) of a sample (15125-74) containing a large fractional volume of crystallites. The strongly temperature-dependent set of profiles in State B indicate that a significant increase in mid-gap defect states has occurred during light soaking. (b) and (d) Show this behavior to be absent in a highly amorphous film (15125-94). Instead, a slight decrease is seen in the drive level profiles between State A and State B. This is most likely attributed to a decrease in the free carrier density during light soaking.

optical spectra described above. Figure 5a and b compare the 3.5-kHz DLCP profiles for two samples, with high and low crystalline fractions, in their fully annealed states. In both cases, the profiles indicate very low density values, which do not increase with increasing temperature up to 350 K. This indicates a very low density of deep defects having thermal emission energies within ~0.65 eV below E_C (via Equation (4)).

Upon light soaking, one would expect the deep defect response to increase and, indeed, there is evidence in Figure 5c for a strong deep defect response in the sample with the lower amorphous fraction. The displayed monotonic increase with measurement temperature indicates a broad defect band, as interpreted by Equation (5). The higher amorphous fraction sample, in contrast, shows no increase in the deep state response: it actually appears to show a slight reduction. The latter may be due to an overall decrease in free electron carriers, as deep states are created by light soaking provided that those states are too deep to respond at 3.5 kHz at

350 K and below. This is in keeping with the behavior of deep defects observed in a-Si:H, since a deep defect response is not observed at 3.5 k Hz for temperatures below ~380 K [11].

The DLCP behavior exhibited in Figure 5, before and after light soaking, for nc-Si:H samples with higher and lower amorphous fractions has been confirmed in many different samples. We believe this to be a general feature of nc-Si:H material produced at United Solar. The key question, therefore, is why such a deep state response makes a strong appearance after light-soaking in samples with higher crystalline fractions (while not in samples with lower fractions).

We believe the schematic diagram in Figure 4 again provides one plausible answer. Transport of electron carriers is expected to occur predominantly in the crystallite phase of these mixed phase samples in all cases. However, for more crystalline samples, these carriers essentially encounter no barrier for capture into a deep defect residing in the amorphous regions, while, in the more amorphous samples, the capture likely occurs via amorphous silicon conduction band states, which presents a significantly larger barrier for carrier capture. Such an explanation, if true, would provide a complementary and consistent model that could account for the different behaviors observed both in the optical spectra and thermal excitations revealed by these DLCP measurements.

5. Discussion and conclusions

It is now well accepted that nc-Si:H is a mixed-phase material which can contain a substantial fraction of a-Si:H. This is readily revealed by Raman spectroscopy, which also allows a rough estimate of the amorphous and crystalline volume fractions. However, evidence for the presence of the amorphous phase is generally occluded in optical spectral measurements owing to the much higher absorption in the crystalline phase above 1.1 eV. Thus, the spectra obtained by, for example, PDS or CPM appear nearly identical to those for microcrystalline Si in which the amorphous phase is nearly absent. In contrast to such measurements, in many nc-Si:H samples, we are able to observe a clear a-Si:H spectral signature using transient photocapacitance (TPC) spectroscopy under certain experimental conditions. This is due to the suppression of the TPC signal from the nanocrystalline phase at higher temperatures owing to its larger hole collection. On the other hand, the a-Si:H-like TPC spectral signature is never observed for samples having amorphous fractions below 40 vol%. Moreover, in certain samples, a negative TPC regime is evident, indicating a strong transition from the valence band into a band of unoccupied deep defect levels. However, the photon energy threshold for these negative TPC regions is quite different depending on the amorphous phase volume fraction. We argued that all of the above observations could be accounted for by hypothesizing that the samples with higher crystalline fractions contain amorphous phase regions which are substantially thinner. This results in a higher degree of quantum mechanical mixing between the electronic levels in the two phases, causing the energy barriers separating the electronic transitions in the amorphous and the crystalline phases to effectively disappear. A schematic illustrating this proposal was presented in Figure 4.

Table 2. Hole collection fractions, f_p, at 300 K determined by the TPC and TPI signal ratios at a photon energy of 1.5 eV for a set of nc-Si:H sample devices of various amorphous volume fractions, X_a. In all cases, the hole collection fractions, f_p, decrease after light soaking. The pre-light-soaked open circuit voltages and efficiencies are included for reference. The highest efficiency sample is the only one listed that was deposited on a textured AgZnO substrate.

Sample	X_a	V_{oc}	Efficiency (%)	f_p^A	f_p^B
16114	0.71	0.568	5.4	0.97	0.42
14657	0.54	N/A	N/A	1.0	0.95
13993	0.47	0.548	8.57	>1.0	0.75
16115	0.23	0.448	4.42	0.98	0.80

Regardless of the crystallite fraction, we found that the relative hole collection, determined by comparing the magnitudes of the TPC and TPI signals at 1.5 eV, decreased substantially after light soaking (see Table 2). The degree of decrease has not yet been determined in many samples and, as yet, appears to be uncorrelated with the measured amorphous fractions. Nonetheless, studies of the spectral dependence of the light-soaking effects in nc-Si:H generally indicate that it is the a-Si:H component which is responsible for the light-induced degradation of cell performance [46].

On the other hand, one of most surprising aspects of light soaking is illustrated by the DLCP results displayed in Figure 5. In essentially every instance, we have found that the nc-Si:H materials with the smaller amorphous fractions show a large light-induced increase in a deep defect acting as a majority carrier trap, while the samples with higher amorphous fraction show no such increase. At first glance, this seems to contradict the idea that the presence of the amorphous phase is responsible for the light-induced effects.

However, we believe that higher amorphous phase samples also undergo a light-induced increase in deep defects, but that this defect band is not revealed in the DLCP measurements. One possible explanation is suggested by our proposed model in Figure 4; namely, that a large barrier separates the free carriers in the crystalline phase from the light-induced defects in the amorphous phase. This prevents the carriers from being trapped and thermally re-emitted at the ~0.1-ms time-scale of the DLCP measurement. In the samples with higher crystalline fractions and thinner amorphous regions, tunneling allows carriers to undergo trapping into these defects directly from the crystallite conduction band. Moreover, the temperature dependence of the deep defect response in those more crystalline samples (see Figure 5c) indicates an activation energy near 0.6 eV, much lower than is encountered in deep trapping of electrons in a-Si:H itself.

While the above argument seems quite plausible and is also supported by the behavior of the observed TPC spectra, there are other ways one might account for the different DLCP results. Perhaps the defect band that appears after light soaking resides at the amorphous/nanocrystallite phase boundaries and these boundaries encompass more potential precursor sites as the nanocrystallite volume fraction increases. Or, perhaps the energy of the light-induced defect lies below the quasi-Fermi level in deep depletion in a higher amorphous fraction sample, so that the

alternating voltage applied during the DLCP measurement is unable to modulate the occupation of that defect. Such explanations cannot yet be ruled out, but can probably be tested by future measurements. Certainly, the electronic processes in nc-Si:H are complex and we can only claim to have begun the process of formulating microscopic models that might account for the surprising features which our TPC and DLCP measurements have revealed.

Acknowledgements

This work was partially supported by NREL under the Thin Film Partnership Program subcontract no. ZXL-6-44205-14 at United Solar and no. ZXL-5-44205-11 at the University of Oregon, and by US DOE under the Solar America Initiative Program Contract no. DE-FC36-07 GO 17053 at both United Solar and the University of Oregon.

Reference:

[1] W.E. Spear and P.G. LeComber, Solid State Commun. 17 (1975) p.1193.
[2] W.E. Spear and P.G. LeComber, J. Non-Cryst. Solid. 8/10 (1972) p.727.
[3] A. Madan, P.G. LeComber and W.E. Spear, J. Non-Cryst. Solid. 20 (1976) p.239.
[4] A.J. Snell, K.D. MacKenzie, P.G. LeComber and W.E. Speas, Phil. Mag. B 40 (1979) p.1.
[5] P. Viktorovitch and G. Moddel, J. Appl. Phys. 51 (1981) p.4847.
[6] M. Hirose, T. Suzuki and G.H. Doehler, Appl. Phys. Lett. 34 (1979) p.234.
[7] J.D. Cohen, D.V. Lang and J.P. Harbison, Phys. Rev. Lett. 45 (1980) p.197.
[8] D.V. Lang, J.D. Cohen and J.P. Harbison, Phys. Rev. B 25 (1982) p.5285.
[9] C.E. Michelson, A.V. Gelatos and J.D. Cohen, Appl. Phys. Lett. 47 (1985) p.412.
[10] K.K. Mahavadi, K. Zellama, J.D. Cohen and J.P. Harbison, Phys. Rev. B 35 (1987) p.7776.
[11] T. Unold, J. Hautala and J.D. Cohen, Phys. Rev. B 50 (1994) p.16985.
[12] J.T. Heath, J.D. Cohen and W.N. Shafarman, J. Appl. Phys. 95 (2004) p.1000.
[13] A.V. Gelatos, J.D. Cohen and J.P. Harbison, Appl. Phys. Lett. 49 (1986) p.722.
[14] A.V. Gelatos, K.K. Mahavadi, J.D. Cohen and J.P. Harbison, Appl. Phys. Lett. 53 (1988) p.403.
[15] C.E. Michelson and J.D. Cohen, Phys. Rev. B 41 (1990) p.1529.
[16] T. Unold and J.D. Cohen, Appl. Phys. Lett. 58 (1991) p.723.
[17] T. Unold, J.D. Cohen and C.M. Fortmann, Appl. Phys. Lett. 64 (1994) p.1714.
[18] F. Zhong, C.-C. Chen and J.D. Cohen, J. Non-Cryst. Solid. 198/200 (1996) p.572.
[19] C.-C. Chen, F. Zhong, J.D. Cohen, J.C. Yang and S. Guha, Phys. Rev. B 57 (1998) p.4210.
[20] S. Guha, X. Xu, J. Yang and A. Banerjee, Appl. Phys. Lett. 66 (1995) p.595.
[21] H. Keppner, J. Meier, P. Torres, D. Fischer and A. Shah, Appl. Phys. A 69 (1999) p.169.
[22] B. Yan, G. Yue, J. Yang, A. Banerjee and S. Guha, Mater. Res. Soc. Symp. Proc. 762 (2003) p.A4.1.1.
[23] J. Yang, B. Yan and S. Guha, Thin Solid Films 487 (2005) p.162.
[24] R.E.I. Schropp, H. Li, R.H. Franken, J.H. Rath, C.H.M. van der Werf, M.A. Schuttauf and R.L. Stolk, Thin Solid Films 516 (2008) p.6818.
[25] B. Yan, G. Yue, J.M. Owens, J. Yang and S. Guha, Appl. Phys. Lett. 85 (2004) p.1925.
[26] G. Yue, B. Yan, J. Yang and S. Guha, J. Appl. Phys. 98 (2005) p.074902.
[27] P.G. Hugger, J.D. Cohen, B. Yan, G. Yue, X. Xu, J. Yang and S. Guha, J. Non-Cryst. Solid. 354 (2008) p.2460.

[28] B. Yan, G. Yue, J.M. Owens, J. Yang and S. Guha, *Conference Record of the 2006 IEEE 4th World Conference on Photovoltaic Energy Conversion*, Hawaii, USA, May 7–12, 2006, p. 1477.
[29] G. Yue, B. Yan, G. Ganguly, J. Yang, S. Guha and C.W. Teplin, Appl. Phys. Lett. 88 (2006) p.263507.
[30] D. Han, J.D. Lorentzen, J. Weinberg-Wolf, L.E. McNeil and Q. Wang, J. Appl. Phys. 94 (2003) p.2930.
[31] E. Bustarret, M.A. Hachicha and M. Brunel, Appl. Phys. Lett. 52 (1988) p.1675.
[32] M. Vanecek, J. Kocka, J. Stuchlik and A. Triska, Solid State Commun. 39 (1981) p.1199.
[33] M. Vanecek, J. Kocka, J. Poruba and A. Fejfar, J. Appl. Phys. 78 (1995) p.6203.
[34] W.B. Jackson and N.M. Amer, Phys. Rev. B 25 (1982) p.5559.
[35] J.D. Cohen and A.V. Gelatos, in *Advances in Amorphous Semiconductors: I. Amorphous Silicon and Related Materials*, H. Fritzsche ed., World Scientific, Singapore, 1988, pp. 475–512.
[36] M. Vanecek, A. Poruba, Z. Remes, N. Beck and M. Nesladek, J. Non-Cryst. Solid. 227/230 (1998) p.967.
[37] U. Kroll, J. Meier, P. Torres, J. Pohl and A. Shah, J. Non-Cryst. Solid. 227/230 (1998) p.68.
[38] A.F. Halverson, J.J. Gutierrez, J.D. Cohen, B. Yan, J. Yang and S. Guha, Appl. Phys. Lett. 88 (2006) p.071920.
[39] J.D. Cohen, T. Unold, A.V. Gelatos and C.M. Fortmann, J. Non-Cryst. Solid. 141 (1992) p.142.
[40] J.M. Essick and J.D. Cohen, Appl. Phys. Lett. 55 (1989) p.1232.
[41] S. Gall, R. Hirschauer, M. Kolter and D. Braunig, Solar Cells 49 (1997) p.157.
[42] J.P. Kleider, A.S. Gudovskikh and P. Roca i Cabarrocas, Appl. Phys. Lett. 92 (2008) p.162101.
[43] J.D. Cohen, in *Density of States from Junction Measurements in Hydrogenated Amorphous Silicon, in Semiconductors and Semimetals*, Vol. 21, J.I. Pankove ed., Academic Press, Orlando, FL, 1984, pp. 9–98.
[44] S.S. Hegedus and E.A. Fagen, J. Appl. Phys. 71 (1992) p.5941.
[45] H. Antoniadis and E.A, Schiff, Phys. Rev. 46 (1992) p.9482.
[46] G. Yue, B. Yan, G. Ganguly, J. Yang and S. Guha, J. Mater. Res. 22 (2007) p.1128.